Direct Observation of Stalled Fork Restart via Fork Regression in the T4 Replication System

Maria Manosas *et al.*

Science **338**, 1217 (2012);
DOI: 10.1126/science.1225437

11. S. S. Chng, L. S. Gronenberg, D. Kahne, *Biochemistry* **49**, 4565 (2010).
12. S. S. Chng, N. Ruiz, G. Chimalakonda, T. J. Silhavy, D. Kahne, *Proc. Natl. Acad. Sci. U.S.A.* **107**, 5363 (2010).
13. E. Freinkman, S. S. Chng, D. Kahne, *Proc. Natl. Acad. Sci. U.S.A.* **108**, 2486 (2011).
14. T. Wu *et al*., *Proc. Natl. Acad. Sci. U.S.A.* **103**, 11754 (2006).
15. M. P. Bos, B. Tefsen, J. Geurtsen, J. Tommassen, *Proc. Natl. Acad. Sci. U.S.A.* **101**, 9417 (2004).
16. P. Sperandeo *et al*., *J. Bacteriol.* **190**, 4460 (2008).
17. L. Wang, A. Brock, B. Herberich, P. G. Schultz, *Science* **292**, 498 (2001).
18. J. W. Chin, A. B. Martin, D. S. King, L. Wang, P. G. Schultz, *Proc. Natl. Acad. Sci. U.S.A.* **99**, 11020 (2002).
19. Y. Ryu, P. G. Schultz, *Nat. Methods* **3**, 263 (2006).
20. C. C. Liu, P. G. Schultz, *Annu. Rev. Biochem.* **79**, 413 (2010).
21. H. R. Kaback, *Methods Enzymol.* **22**, 99 (1971).
22. H. R. Kaback, E. R. Stadtman, *Proc. Natl. Acad. Sci. U.S.A.* **55**, 920 (1966).
23. Y. J. Kim, T. Rajapandi, D. Oliver, *Cell* **78**, 845 (1994).
24. T. Yakushi, N. Yokota, S. Matsuyama, H. Tokuda, *J. Biol. Chem.* **273**, 32576 (1998).
25. See supplementary materials on *Science* Online.
26. S. Murakami, R. Nakashima, E. Yamashita, T. Matsumoto, A. Yamaguchi, *Nature* **443**, 173 (2006).
27. H. Nikaido, *Annu. Rev. Biochem.* **78**

References and Notes

1. C. R. Raetz, C. Whitfield, *Annu. Rev. Biochem.* **71**, 635 (2002).
2. N. Ruiz, L. S. Gronenberg, D. Kahne, T. J. Silhavy, *Proc. Natl. Acad. Sci. U.S.A.* **105**, 5537 (2008).
3. P. Sperandeo *et al*., *J. Bacteriol.* **189**, 244 (2007).
4. N. Ruiz, D. Kahne, T. J. Silhavy, *Nat. Rev. Microbiol.* **7**, 677 (2009).
5. S. Narita, H. Tokuda, *FEBS Lett.* **583**, 2160 (2009).
6. E. Freinkman, S. Okuda, N. Ruiz, D. Kahne, *Biochemistry* **51**, 4800 (2012).
7. P. Sperandeo *et al*., *J. Bacteriol.* **193**, 1042 (2011).
8. M. D. Suits, P. Sperandeo, G. Dehò, A. Polissi, Z. Jia, *J. Mol. Biol.* **380**, 476 (2008).
9. A. X. Tran, C. Dong, C. Whitfield, *J. Biol. Chem.* **285**, 33529 (2010).
10. M. Braun, T. J. Silhavy, *Mol. Microbiol.* **45**, 1289 (2002).

fork regression to bypass leading-strand lesions via an active helicase-driven pathway involving the UvsW protein (*5*). UvsW is a functional analog of *E. coli* RecG helicase and has properties similar to those of the RecQ helicase family, which includes human enzymes whose defects contribute to various disease states (*8*–*10*). With its dual unwinding and annealing activities (*11*), UvsW is capable of regressing forks in vitro (*5*, *6*). In the T4 system, when the replisome encounters a leading-strand lesion, replication in the lagging strand continues at least one Okazaki fragment beyond the lesion site (*6*). This uncoupled synthesis results in a DNA structure that can be effectively regressed by UvsW helicase to generate the HJ structure required for template switching (fig. S1). However, the reconstruction of the full template-switching pathway is missing.

We investigated lesion bypass via template switching, using magnetic tweezers to manipulate a DNA hairpin and follow the activity of the UvsW helicase alone and in collaboration with different components of the replisome. Experiments were carried out by tethering the DNA hairpin between a glass surface and a magnetic bead (Fig. 1A). A pair of magnets was used to apply tension to the ends of the hairpin, while the extension of the DNA molecule $Z_e(t)$ was obtained from tracking the position of the bead (*12*). Three different hairpins provided either adapted sequences or modified bases (fig. S2): 7-Kbp long (Lh), 1.2-Kbp medium (Mh), and 100-bp short (Sh) hairpins. By applying a force of ~15 pN, we trapped Mh molecules in an intermediate configuration in which the initial stem was denatured but the GC-rich region before the apex remained intact (fig. S2D). This partially denatured hairpin was an ideal substrate to simultaneously test UvsW annealing and unwinding activities (Fig. 1B). The changes in $Z_e(t)$ were converted to the number of unwound or annealed base pairs, using the single-stranded DNA (ssDNA) elasticity (fig. S3).

In the presence of UvsW and adenosine triphosphate (ATP), we observed events corresponding to the zipping of the hairpin, followed by the spontaneous recovery of the initial molecular extension (Fig. 1C). After the annealing burst, UvsW remained bound, maintaining the formed hairpin for a fraction of a second before dissociating. The rate of annealing and the enzyme's processivity measured at 15 pN were very large: ~1300 bp/s and ~9 Kbp, respectively (Fig. 1D and fig. S4). UvsW annealing activity was also tested with an ensemble fluorescence resonance energy transfer–based assay (fig. S5). We found that the UvsW annealing activity is an active process that requires ATP hydrolysis, with a Michaelis constant and catalytic constant of 57 μM and 1280 bp/s, respectively (fig. S6). Unwinding by UvsW was observed only when annealing was prevented (closed hairpin at low forces, fig. S7) or in resolving branched structures requiring combined annealing and unwinding activities (fig. S8). These results showed that UvsW possessed both unwinding and annealing activities, but favored annealing.

Ensemble kinetic studies using a synthetic branched HJ (*13*) confirmed that UvsW resolved branched structures efficiently (fig. S9). To investigate in real time the generation and migration of an HJ by UvsW with magnetic tweezers, we constructed a DNA substrate mimicking a stalled fork (Fig. 2A) in situ by using either a Mh or Lh (figs. S2 and S10A). The fork regression was then initiated by introducing UvsW and ATP. HJ migration was followed by monitoring changes in $Z_e(t)$ (Fig. 2B). The transient decreases and increases in $Z_e(t)$ corresponded to the migration of the formed HJ in the downward and upward directions. By using double-stranded DNA (dsDNA) elasticity (fig. S3), we converted $Z_e(t)$ into migrated base pairs and measured a rate of HJ migration close to the annealing rate, 1000 to 1300 bp/s, with a small force-dependent asymmetry between the branch migration rates against or favored by the applied force (Fig. 2C and fig. S10). Frequent instantaneous random switches in the migration direction, mediated by a single enzyme complex (figs. S11 and S12), were observed with a characteristic time of ~2 s (Fig. 2D). The ability of UvsW to switch migration direction is essential during the remodeling of stalled forks, because it provides the means to revert the HJ back to a normal fork.

The template-switching pathway (fig. S1) requires the coordinated action of several proteins. We investigated whether the minimal system consisting of UvsW and the T4 holoenzyme [composed of gp43 polymerase, a gp45 sliding clamp, and a gp44/62 clamp loader (*14*)] was sufficient to reproduce such a pathway in vitro. Ensemble experiments on a plasmid substrate had shown that a lesion in the leading strand regressed a fork by the minimal protein system (*6*).We prepared a stalled fork substrate presenting a lesion on the leading strand (Fig. 3A), using a 100-bp hairpin with a built-in primer (fig. S13), which contained three locked nucleic acid (LNA) nucleotides in the template leading strand (40 bp before the apex), presenting an efficient roadblock for the holoenzyme (*15*) that arrested 98% of the molecules (Fig. 3C).

The addition of UvsW, T4 holoenzyme, ATP, and nucleotides first produced a transient decrease associated with fork regression, and next an increase associated with the recovery of the replication fork (Fig. 3B). When the HJ structure

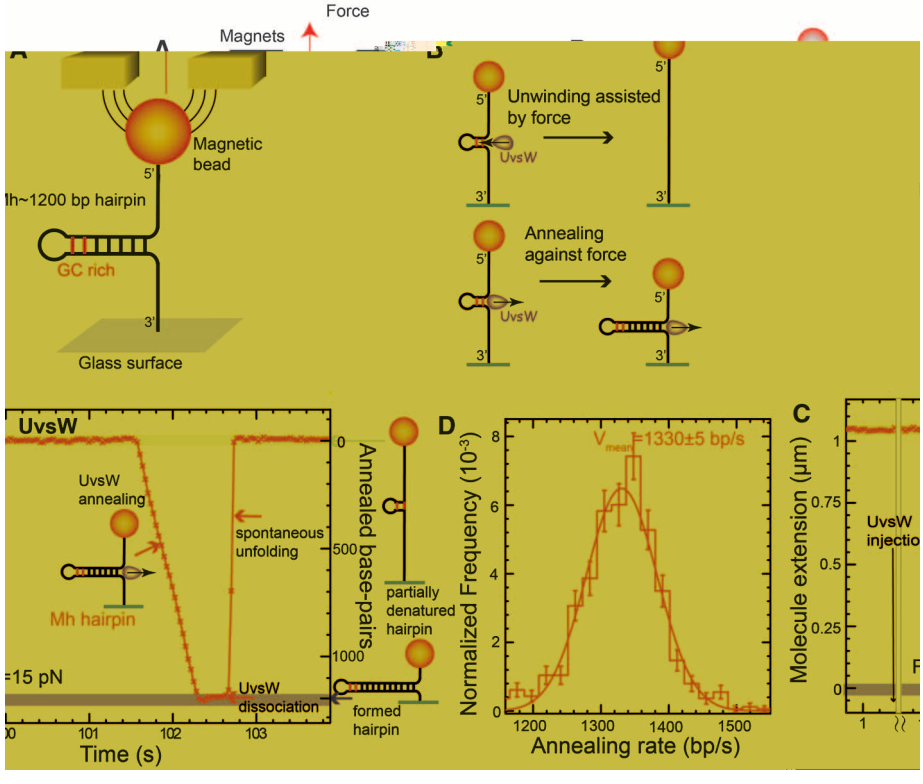

Fig. 1. Single-molecule characterization of UvsW annealing activity. (**A**) Schematic representation of the experimental setup. A DNA hairpin substrate was tethered between the glass surface and a magnetic bead held in a magnetic trap (MT). The GC-rich region in the Mh is shown in red. (**B**) Schematics of the assay allowing for unwinding and annealing detection. (**C**) Experimental trace showing $Z_e(t)$ obtained in the MT assays with the partially denatured hairpin at a force (*F*) of 15 pN with ATP and UvsW. Annealing bursts were detected as decreases in Z_e. (**D**) Distribution of annealing rates dZ_e/dt (n = 766 events) with a Gaussian fit. Error bars are inversely proportional to the square root of the number of points for each bin.

is formed, the holoenzyme has the ability to extend the leading strand using the exogenous oligonucleotide as the template. We did not directly detect this initial elongation of the primer, because it was not associated with a change in $Z_e(t)$, but its further extension by the holoenzyme after fork progression by UvsW had restored the fork, with the LNA lesion bypassed (Fig. 3B). Template switching and final hairpin synthesis were further confirmed by checking the disappearance of spontaneous fluctuations of the hairpin caused by its conversion to a full DNA duplex (fig. S14). The frequency of full replicated substrates was increased by more than a factor of 30 in the presence of UvsW (Fig. 3C), confirming the need for fork regression and thus demonstrating the template-switching process in vitro. The fact that the time required for lesion bypass (~0.3 s) was much smaller than the typical holoenzyme loading time (~20 s) (fig. S15) suggests that the holoenzyme probably remained bound to execute both HJ primer extension and final strand displacement synthesis. The random switching of UvsW between fork regression and progression appears to be a simple means to coordinate its action with the holoenzyme, without the need for a strict synchronization mechanism.

How does UvsW coordinate its action with the different replisome components so as not to interfere with the normal replication process? First, we tested the effect of T4 gp32 ssDNA binding protein (*16*) on UvsW activity on a partially denatured hairpin. Normal annealing activity was detected in those assays (fig. S16), demonstrating the ability of UvsW to catalyze protein displacement. Next, we performed competition experiments between UvsW and the holoenzyme and/or replicative helicase. We found that UvsW annealed a partially replicated hairpin even when the T4 holoenzyme was replicating the leading strand, supporting the hypothesis that UvsW annealing promotes the shift of the leading-strand holoenzyme from the fork to the formed HJ (fig. S17A). In contrast, no UvsW activity was detected when the replicative helicase (*17*) was unwinding the dsDNA (moving along the lagging strand), isolated from or coupled to the T4 holoenzyme during leading-strand synthesis (fig. S17, B and C), demonstrating that gp41 helicase dissociation was required for initiation of the UvsW-catalyzed reversal. Thus, UvsW activity was inhibited during coupled replication (fig. S17D). Blockage of the leading-strand holoenzyme at the lesion site leads to the helicase uncoupling from the holoenzyme and to helicase dissociation [fig. S18 and (*6*)], then allowing for UvsW loading.

Following the activities of UvsW together with those of the replisome, we have reconstructed the steps for the complete template-switching pathway in vitro. The overall results provide the basis for a stepwise model of a lesion bypass mechanism in T4 (fig. S19): (i) DNA lesion–induced partial uncoupling of the replisome, which allows UvsW loading after the departure of the helicase; (ii) fork regression by UvsW, shifting the leading-strand holoenzyme to the formed HJ; (iii) leading-strand primer extension by the holoenzyme while UvsW is migrating the HJ; (iv) UvsW randomly switching direction; and (v) fork progression by UvsW to recover the replication fork where the lesion is now bypassed. Several helicases, such as *E. coli* RecG or human BLM and WRN

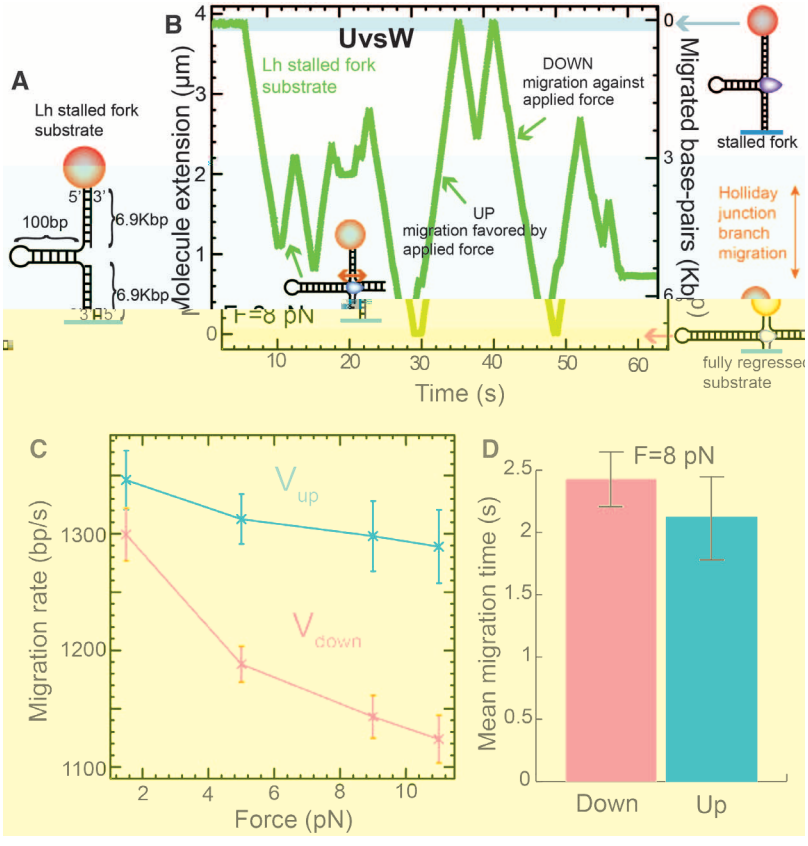

Fig. 2. Single-molecule characterization of UvsW HJ migration activity. (**A**) Schematics of the Lh stalled fork substrate. (**B**) Experimental HJ migration trace showing $Z_e(t)$ with the Lh stalled fork substrate, ATP, and UvsW at F = 8 pN. (**C**) Mean HJ migration rate measured in the downward (against the applied force) and upward (favored by the applied force) migration directions as a function of the applied force (n = 54 to 248 events). Error bars are SEM. (**D**) Mean migration time in the downward and upward directions (n = 69 events). Error bars are SEM.

Fig. 3. Reconstruction of the template-switching pathway. (**A**) Sh stalled fork substrate with a LNA block at the leading strand. (**B**) Experimental trace at F = 8 pN showing $Z_e(t)$ with ATP, dNTPs, UvsW, and the T4 holoenzyme, starting with the stalled fork and ending with the fully replicated substrate. (**C**) Frequency of events showing the full synthesis of the hairpin in the presence (n = 58 events) and absence (n = 95 events) of UvsW. Error bars are SEM.

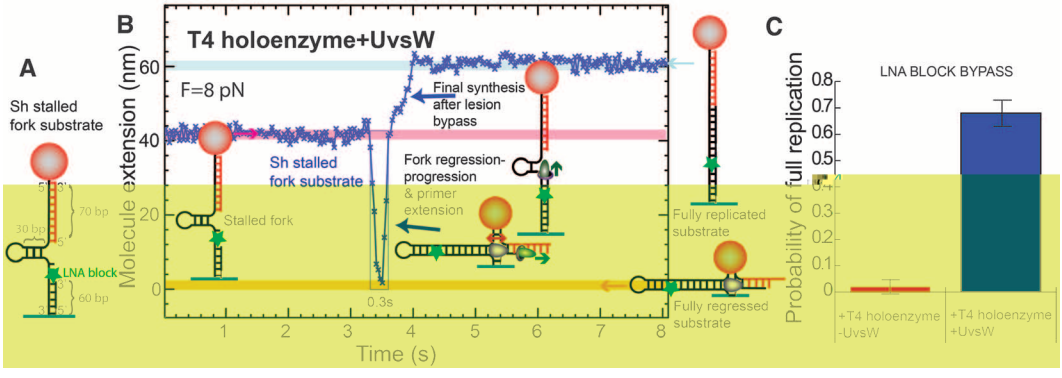

helicases, have the ability to remodel stalled forks (*18*, *19*) and can potentially play the role of UvsW in fork regression pathways in *E. coli* and human cells, respectively.

References and Notes

1. M. M. Cox *et al.*, *Nature* **404**, 37 (2000).
2. J. Atkinson, P. McGlynn, *Nucleic Acids Res.* **37**, 3475 (2009).
3. N. P. Higgins, K. Kato, B. Strauss, *J. Mol. Biol.* **101**, 417 (1976).
4. Y. Fujiwara, M. Tatsumi, *Mutat. Res. Fundam. Mol. Mech. Mugag.* **37**, 91 (1976).
5. D. T. Long, K. N. Kreuzer, *EMBO Rep.* **10**, 394 (2009).
6. S. W. Nelson, S. J. Benkovic, *J. Mol. Biol.* **401**, 743 (2010).
7. J. T. P. Yeeles, K. J. Marians, *Science* **334**, 235 (2011).
8. K. Carles-Kinch, J. W. George, K. N. Kreuzer, *EMBO J.* **16**, 4142 (1997).
9. A. E. Gorbalenya, E. V. Koonin, A. P. Donchenko, V. M. Blinov, *Nucleic Acids Res.* **17**, 4713 (1989).
10. W. K. Chu, I. D. Hickson, *Nat. Rev. Cancer* **9**, 644 (2009).
11. S. W. Nelson, S. J. Benkovic, *J. Biol. Chem.* **282**, 407 (2007).
12. C. Gosse, V. Croquette, *Biophys. J.* **82**, 3314 (2002).
13. M. R. Webb, J. L. Plank, D. T. Long, T. S. Hsieh, K. N. Kreuzer, *J. Biol. Chem.* **282**, 34401 (2007).
14. K. J. Hacker, B. M. Alberts, *J. Biol. Chem.* **269**, 24221 (1994).
15. M. Manosas *et al.*, *Nucleic Acids Res.* **40**, 6174 (2012).
16. J. W. Chase, K. R. Williams, *Annu. Rev. Biochem.* **55**, 103 (1986).
17. M. Venkatesan, L. L. Silver, N. G. Nossal, *J. Biol. Chem.* **257**, 12426 (1982).
18. P. McGlynn, R. G. Lloyd, *Proc. Natl. Acad. Sci. U.S.A.* **98**, 8227 (2001).
19. A. Machwe, L. Xiao, J. Groden, D. K. Orren, *Biochemistry* **45**, 13939 (2006).

Acknowledgments: We thank B. Michel and D. Bensimon for useful comments on the manuscript and M. M. Spiering for DNA substrates. This work was supported by a Human Frontier Science Program grant (to V.C. and S.J.B.), U.S. National Institutes of Health grant GM013306 (to S.J.B.), ERC grant Magreps 267 862 (to V.C.), and Juan de la Cierva Program MICINN-JDC (to M.M). M.M. conducted single-molecule assays and performed the analysis. S.K.P. conducted ensemble assays, analyzed data, and prepared DNA and proteins. V.C. built the magnetic tweezers. M.M., S.K.P., V.C., and S.J.B. wrote the paper. Materials and methods are available as supplementary materials.

Supplementary Materials

www.sciencemag.org/cgi/content/full/338/6111/1217/DC1
Materials and Methods
Figs. S1 to S19
Table S1
References (*20*–*28*)

31 May 2012; accepted 17 October 2012
10.1126/science.1225437

Progenitor and Terminal Subsets of CD8$^+$ T Cells Cooperate to Contain Chronic Viral Infection

Michael A. Paley,[1] Daniela C. Kroy,[2] Pamela M. Odorizzi,[1] Jonathan B. Johnnidis,[1] Douglas V. Dolfi,[1] Burton E. Barnett,[1] Elizabeth K. Bikoff,[3] Elizabeth J. Robertson,[3] Georg M. Lauer,[2] Steven L. Reiner,[4]* E. John Wherry[1]†

Chronic infections strain the regenerative capacity of antiviral T lymphocyte populations, leading to failure in long-term immunity. The cellular and molecular events controlling this regenerative capacity, however, are unknown. We found that two distinct states of virus-specific CD8$^+$ T cells exist in chronically infected mice and humans. Differential expression of the T-box transcription factors T-bet and Eomesodermin (Eomes) facilitated the cooperative maintenance of the pool of antiviral CD8$^+$ T cells during chronic viral infection. T-bet^{hi} cells displayed low intrinsic turnover but proliferated in response to persisting antigen, giving rise to Eomes^{hi} terminal progeny. Genetic elimination of either subset resulted in failure to control chronic infection, which suggests that an imbalance in differentiation and renewal could underlie the collapse of immunity in humans with chronic infections.

Lifelong immunity to acutely resolved infections requires maintenance of memory lymphocytes that, upon reinfection, regenerate a large cohort of short-lived, terminal progeny while concurrently replenishing the long-lived memory pool. During low-level latent/reactivating infections, such as cytomegalovirus (CMV), this periodic replenishment of short-lived and long-lived populations is balanced to achieve lifelong immunity. Chronic viral infections with prolonged and elevated antigen load, however, may strain the renewal capacity of long-lived lymphocytes by persistent elicitation of short-lived cells. For example, increased CD8$^+$ T cell turnover is observed during HIV infection (*1*–*3*). This stems from an elevated production of short-lived cells and a concurrent reduction in the long-lived pool (*4*) and is thought to underlie the eventual collapse of adaptive immunity during HIV infection. It is unclear, however, which molecular pathways govern the renewal and differentiation of virus-specific CD8$^+$ T cells during chronic infections, or whether these antiviral responses are sustained by a progenitor-progeny relationship.

Two T-box transcription factors, T-bet and Eomesodermin (Eomes), regulate both functional and dysfunctional CD8$^+$ T cell responses (*5*–*10*). During chronic viral infections, T-bet is reduced in virus-specific CD8$^+$ T cells, and this reduction correlates with T cell dysfunction (*9*–*11*). In contrast, microarray analysis of CD8$^+$ T cells suggested that Eomes mRNA is elevated during chronic infection (*12*). Using acute or chronic infection with lymphocytic choriomeningitis virus (LCMV), we found that Eomes expression was up-regulated in exhausted CD8$^+$ T cells during chronic infection (Fig. 1, A to C, and fig. S1A).

In contrast to acute infection, T-bet and Eomes were reciprocally expressed in exhausted CD8$^+$ T cells by day 15 to day 30 of chronic infection (Fig. 1D). In addition, Eomes-expressing CD8$^+$ T cells had higher expression of Blimp-1 and several inhibitory receptors (Fig. 1, E and F, and fig. S1B), consistent with more severe exhaustion (*13*–*17*). Furthermore, Eomes^{hi} virus-specific CD8$^+$ T cells had less co-production of interferon-γ (IFN-γ) and tumor necrosis factor–α (TNF-α) (*16*, *18*) (fig. S1C). However, high expression of Eomes or the inhibitory receptor PD-1 correlated with increased granzyme B and cytotoxicity, despite lower degranulation (fig. S1, D to H). Thus, Eomes expression in virus-specific CD8$^+$ T cells during chronic infection was associated with markers of severe exhaustion and reduced co-production of antiviral cytokines, despite better cytotoxicity than T-bet^{hi} cells.

Although wild-type CD8$^+$ T cells had bimodal expression of T-bet and Eomes, genetic deletion of T-bet resulted in increased Eomes and PD-1 expression (Fig. 1G) (*9*). In contrast, Eomes-deficient CD8$^+$ T cells had reduced PD-1 and Blimp-1, as well as increased T-bet and cytokine co-production (Fig. 1, G to I, and fig. S2). Thus, T-bet and Eomes support separate subpopulations of virus-specific CD8$^+$ T cells during chronic infection.

To determine the relative contribution of these T-bet^{hi} and Eomes^{hi} CD8$^+$ T cell subsets to the magnitude of the response during chronic infection, we quantified these populations in multiple anatomical locations. Overall, the Eomes^{hi} population outnumbered the T-bet^{hi} population by a factor of ~20 (fig. S3A), and these subsets had distinct tissue distribution (fig. S3, B and C). As observed in intact mice, sorted and adoptively transferred PD-1^{int} (T-bet^{hi}) cells preferentially accumulated in the spleen, whereas PD-1^{hi}

[1]Department of Microbiology and Institute for Immunology, Perelman School of Medicine, University of Pennsylvania, Philadelphia, PA 19104, USA. [2]Gastrointestinal Unit, Massachusetts General Hospital, Harvard Medical School, Boston, MA 02115, USA. [3]Sir William Dunn School of Pathology, University of Oxford, Oxford OX1 3RE, UK. [4]Department of Medicine, Abramson Family Cancer Research Institute, and Institute for Immunology, Perelman School of Medicine, University of Pennsylvania, Philadelphia, PA 19104, USA.

*Present address: Department of Microbiology and Immunology and Department of Pediatrics, College of Physicians and Surgeons of Columbia University, New York, NY 10032, USA. †To whom correspondence should be addressed. E-mail: wherry@mail.med.upenn.edu